Journal of Power Sources 262 (2014) 279–285

Contents lists available at ScienceDirect

Journal of Power Sources

journal homepage: www.elsevier.com/locate/jpowsour

Synthesis of Pt–Pd bimetallic nanoparticles anchored on graphene for highly active methanol electro-oxidation

Yuting Zhang [a], Gang Chang [a,*], Honghui Shu [a], Munetaka Oyama [b], Xiong Liu [a], Yunbin He [a,*]

[a] Hubei Collaborative Innovation Center for Advanced Organic Chemical Materials, Ministry-of-Education Key Laboratory for the Green Preparation and Application of Functional Materials, Faculty of Materials Science and Engineering, Hubei University, No. 368 Youyi Avenue, Wuchang, Wuhan 430062, China
[b] Department of Material Chemistry, Graduate School of Engineering, Kyoto University, Nishikyo-ku, Kyoto 615-8520, Japan

HIGHLIGHTS

- Pt–Pd nanoparticles/graphene (Pt–PdNPs/G) was synthesized within one-step process.
- Environment friendly ascorbic acid was chosen as the reductant.
- The synthesized Pt–PdNPs/G exhibits superior electrocatalytic activity and stability towards electro-oxidation of methanol.
- The best Pt–Pd ratio of Pt–PdNPs/G for methanol oxidations in alkaline condition belongs to 1/3.

ARTICLE INFO

Article history:
Received 22 November 2013
Received in revised form
15 February 2014
Accepted 26 March 2014
Available online 3 April 2014

Keywords:
One-step reduction
Graphene sheets
Bimetallic Pt–Pd nanoparticles
Methanol electro-oxidation

ABSTRACT

A simple, one-step reduction route was employed to synthesize bimetallic Pt–Pd nanoparticles (Pt–PdNPs) supported on graphene (G) sheets, in which the reduction of graphite oxide and metal precursor was carried out simultaneously using ascorbic acid as a soft reductant. The morphology and structure of Pt–PdNPs/G composites were characterized using X-ray diffraction, Transmission Electron Microscopy, Field Emission Scanning Electron Microscopy and X-ray Photoelectron Spectroscopy analysis. The results show that Pt–Pd bimetallic nanoparticles were successfully synthesized and evenly anchored on the graphene sheets. Electrochemical experiments, including cyclic voltammetry and chronoamperometric measurements, were performed to investigate the electrochemical and electrocatalytic properties of the Pt–PdNPs/G composites. It was found that Pt–PdNPs/G composites show better electrocatalytic activity and stability towards the electro-oxidation of methanol than its counterparts such as composites composed of graphene-supported monometallic nanoparticles (PtNPs/G, PdNPs/G) and free-standing (Pt–PdNPs) and Vulcan-supported bimetallic Pt–Pd nanoparticles (Pt–PdNPs/V). The results could be attributed to the synergetic effects of the Pt–Pd nanoparticles and the enhanced electron transfer of graphene. The electrocatalytic activity of Pt–PdNPs/G changed with the Pd content in the Pt–Pd alloy, and the best performance was achieved with a Pt–Pd ratio of 1/3 in an alkaline environment. Our study indicates the potential use of Pt–PdNPs/G as new anode catalyst materials for direct methanol fuel cells.

1. Introduction

Direct methanol fuel cells (DMFCs) are considered a promising power source for a variety of portable applications due to the simplicity of the system, environmental sustainability and a high energy-conversion efficiency [1,2]. However, there are still several challenges hindering the commercial application of DMFCs, including the poisoning effect of intermediates, insufficient durability and high cost of the commonly used Pt catalysts. Thus, the development of new anodic catalysts to improve the cell performance is an urgent need. Combining Pt with another metal to fabricate a bimetallic catalyst is one of the most effective ways to resolve the above problems [3]. The introduction of another metal can significantly reduce the required Pt loading and modify the strength of surface adsorption by changing the d-band structure of

* Corresponding authors. Tel./fax: +86 27 88661803.
E-mail addresses: gchanghubei@gmail.com (G. Chang), ybhe@hubu.edu.cn (Y. He).

http://dx.doi.org/10.1016/j.jpowsour.2014.03.127
0378-7753/

Pt. In particular, the addition of a second or even third metal could adsorb active oxygen species, which can effectively oxidize the intermediates, such as CO-like species adsorbed on the surface, and improve the poisoning resistance and durability of the catalyst [4–11]. To date, a large amount of bimetallic materials with synergistically enhanced performances have been studied based on Pt in combination with its neighboring transition metals, such as Pt–Au [12–14], Pt–Ag [15,16], Pt–Ni [17,18], Pt–Ru [19,20] and Pt–Pd [5,7–9,21]. Among these materials, the Pt–Pd catalyst is more stable than the other bimetallic catalysts at high potentials [3]. Moreover, Pd is 50 times more abundant on earth than Pt and exhibits similar catalytic performance with a higher resistance to intermediate poisoning than Pt during methanol electro-oxidation [22]. In addition, in the previous studies, Pt–Pd bimetallic systems exhibited significantly improved catalytic performance compared to monometallic catalysts and unique characteristics that were not merely the sum of properties of the two constituent metals [7–9]. Thus, bimetallic Pt–Pd catalysts are considered to be the most suitable substitute for Pt catalysts in DMFCs.

To further reduce the usage of noble metals and improve the activity of the catalysts, it is highly desirable to load the bimetallic Pt–Pd nanoparticles onto suitable supporting materials. Graphene, a two-dimensional carbon material with a single or several atomic layers, is considered an excellent support material due to the large surface area, high chemical stability and good electrical conductivity [23]. Recently, considerable efforts have been made to synthesize graphene-supported metal electrocatalysts [23,24], especially Pt–Pd alloys/graphene, to explore their performance in DMFCs. It was found that the loading of metal nanoparticles onto graphene can lead to nanocomposites with larger active surface areas that exhibit higher activity for the methanol electric-oxidation reaction than those on other types of carbon support materials [21,25].

Although Pt–Pd bimetallic nanoparticles anchored on graphene have received a lot of interest from researchers, there is still a lack of facile routes for the synthesis. To date, microwave-assisted methods and electro-deposition methods are the widely accepted preparation methods for the synthesis of Pt–Pd bimetallic catalysts [3,8,21]. However, most of these methods involve with stepwise procedures, indicating a high degree of complexity. In the previous studies [26,27], we reported a simple one-step method for the synthesis of Pt nanoclusters and Pd nanoparticles supported on graphene sheets using ascorbic acid as the reductant. Ascorbic acid is nontoxic, has a mild reductive ability, and provides a method not only to reduce the GO and metal precursors but also to simultaneously stabilize the reduced GO by avoiding the formation of irreversible agglomerates via weakening the strong $\pi-\pi$ stacking tendency between graphene sheets [28]. Likewise, this method can be applied to the synthesis of bimetallic Pt–Pd nanoparticles anchored on graphene sheets.

In this study, well-dispersed Pt–Pd nanoparticles anchored on graphene sheets (Pt–PdNPs/G) were successfully prepared using a simple one-pot process, in which the reduction of graphite oxide and metal precursors was accomplished simultaneously using ascorbic acid as a soft reductant. The synthesized Pt–PdNPs/G composites were characterized using various techniques, including transmission electron microscopy (TEM), field-emission scanning electron microscopy (FE-SEM), X-ray diffraction (XRD) and X-ray photoelectron spectroscopy (XPS). Then, the catalytic activity and tolerance of the Pt–PdNPs/G composites towards methanol oxidation were investigated and compared to those of graphene supported monometallic nanoparticles (PtNPs/G, PdNPs/G) and bimetallic Pt–Pd nanoparticles with no (Pt–PdNPs) or a carbon black (Vulcan) support (Pt–PdNPs/V). Furthermore, the electrocatalytic activities of Pt–PdNPs/G catalysts with different Pt–Pd atomic ratios were investigated, and the optimal Pt–Pd atomic ratio for achieving best electrocatalytic performance towards methanol oxidation was determined. All the results show a great potential of using Pt–PdNPs/G as new anode catalysts in DMFCs.

2. Experimental

2.1. Chemicals

Potassium chloroplatinite (II) (K_2PtCl_4) and potassium tetrachloropalladate (II) (K_2PdCl_4) were purchased from Aldrich Chem. Co. Graphite was obtained from Alfa Aesar. Vulcan XC-72 was purchased from Cabot Corp, and 5 wt% Nafion was ordered from DuPont. Ascorbic acid, Sulfuric acid, *N*,*N*-Dimethylformamide (DMF), $KMnO_4$, $K_2S_2O_8$ and P_2O_5 were purchased from Sinopharm Chemical Reagent Co. All chemicals were analytically pure and used as received without further purification. The deionized pure water for solution preparation was produced from a Kertone Ultrapure Water System P60-CY (Kertone Water Treatment Co. Ltd, resistivity >18 MΩ cm).

2.2. Apparatus

XRD analysis of the as-synthesized samples was carried out using a D8-Advance diffractometer (Bruker, Germany) with a Cu Kα radiation source ($\lambda = 0.15418$ nm). The morphology and structure of the samples were characterized using FE-SEM (ZEISS, Germany) and TEM (FEI TECNAI20, USA). The EDS analysis of the chemical composition was performed with the analyzer coupled to SEM. X-ray photoelectron spectra were recorded using a SPeCS system (PHOIBOS 150, Germany) with Al Kα radiation ($h\nu = 1486.6$ eV). Thermogravimetric analysis (TGA) was performed using a thermogravimetric analyzer (Perkin–Elmer TGA-7, USA). All electrochemical measurements were conducted using a 550 electrochemical workstation (Gaoss Union Instrument Company, China) at room temperature in a conventional three-electrode system with a Pt (wire) counter electrode and an Ag/AgCl reference electrode. Before each experiment, pure N_2 gas was bubbled through the solution to remove any dissolved oxygen.

2.3. Procedures for preparing Pt–PdNPs/G and analog nanocomposites

The graphite oxide (GO) powders were prepared from graphite using the modified Hummers' method [29]. To synthesize the Pt–PdNPs/G, 25 mg GO was first dissolved in 50 mL pure water and exfoliated using ultrasonic treatment for 1 h to achieve well dispersion. Then, 1 mL of 0.01 M K_2PtCl_4 and 1 mL of 0.01 M K_2PdCl_4 (metal precursors in the case of Pt/Pd = 1/1) were mixed with 48 mL pure water. Next, the resulting solution was mixed with the above dispersion, followed by the addition of 500 mg ascorbic acid as the reductant. The mixture was then stirred for 6 h at a temperature of 85 °C under reflux conditions. Finally, solid powders were collected via centrifugation, sequentially washed with double-distilled water and ethanol for several cycles, and dried at 60 °C in a vacuum oven for 12 h; the Pt_1Pd_1NPs/G composite was then obtained. Pt–PdNPs/G composites with various Pt/Pd ratio were synthesized by the same procedure but applying different nominal Pt/Pd ratios in the metal precursors. As reported later, the Pt/Pd ratio in the final Pt–PdNPs/G composite deviates somewhat from the nominal ratio in the initial metal precursors. For clarity and simplicity, however, we use the nominal Pt/Pd ratio for noting the final product of Pt–PdNPs/G throughout the paper. For comparison purposes, graphene-supported monometallic nanoparticles (PtNPs/G and PdNPs/G) were also prepared using the same

procedure but with only the respective single-metal precursor. Bimetallic nanocomposites Pt–PdNPs and Pt–PdNPs/V were synthesized as well via similar procedure with no support and with Vulcan XC-72 (V) as supporting material, respectively. By TGA, the metal loading amounts were calculated to be 67.4% in Pt_1Pd_3NPs/G, 56.4% in PtNPs/G, 71.8% in PdNPs/G and 69.5% in Pt_1Pd_3NPs/V.

2.4. Fabrication of PdNPs/G, PtNPs/G and Pt–PdNPs/G working electrodes

The working electrodes were independently fabricated as follows. First, a glassy carbon (GC) disk (diameter = 3 mm) electrode was polished with slurry of 1, 0.3 and 0.05 μm alumina to mirror finish, rinsed with pure water and dried at room temperature in a vacuum oven for hours. Then, 6 mg of Pt–PdNPs/G composite was dispersed in 1 mL of DMF using ultrasonic treatment to form a homogeneous black suspension. 5 μL of the catalyst suspension was carefully pipetted onto the surface of the GC disc. Finally, 10 μL of 0.5 wt% Nafion was transferred evenly onto the surface of the dry Pt–PdNPs/G and dried at room temperature to form a layer that prevented the catalyst particles from detaching. The as-prepared Pt–PdNPs/G working electrodes were for electrochemical evaluations. PtNPs/G, PdNPs/G, Pt–PdNPs and Pt–PdNPs/V working electrodes were prepared using the same procedure described above.

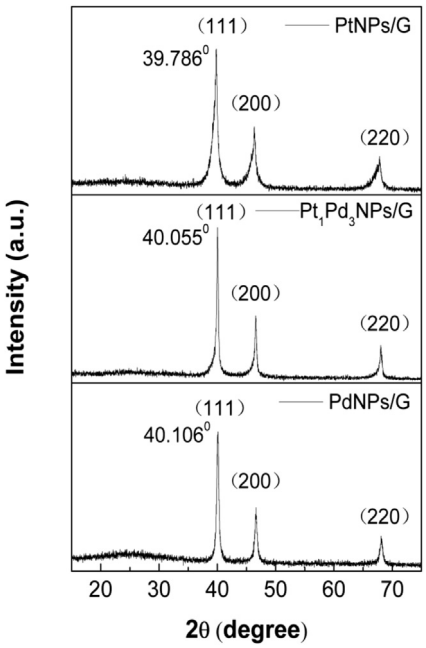

Fig. 1. XRD patterns of PtNPs/G, Pt1Pd3NPs/G, and PdNPs/G nanocomposites.

3. Results and discussion

3.1. Characterization of the morphology and structure of Pt–PdNPs/G and analog nanocomposites

As will be presented later, the Pt–PdNPs/G catalyst with a Pt/Pd ratio of 1/3, i.e., Pt_1Pd_3NPs/G, exhibits the best electrocatalytic performance toward methanol oxidation, therefore, we restrict the following report to Pt_1Pd_3NPs/G in comparison with graphene-supported monometallic (PtNPs/G and PdNPs/G) as well as free-standing and Vulcan–supported bimetallic (Pt_1Pd_3NPs and Pt_1Pd_3NP/V) systems.

To investigate the crystalline phase structure, the as-synthesized Pt–PdNPs/G, PtNPs/G, and PdNPs/G nanocomposites were characterized using XRD measurements. As shown in Fig. 1, a weak and broad peak with 2θ in the range of 20°–30° could be attributed to the reduced graphene support. Pt and PdNPs show peaks that correspond to the (111), (200) and (220) crystal planes of the face-centered cubic (fcc) Pt (JCPDS No. 04-0802) and Pd (JCPDS No. 46-1043), respectively. Similarly, diffraction peaks at 2θ values of 40.05°, 46.56°, and 68.01° are assigned to the (111), (200) and (220) crystal planes of the Pt–PdNPs in the Pt_1Pd_3NPs/G composite. When viewing the (111) peaks more closely, it is evident that Pt_1Pd_3NPs show a single peak at 2θ of 40.04° which is in between the peaks of fcc Pt (39.78°) and fcc Pd (40.10°), confirming the formation of Pt–Pd alloy with also a fcc structure [30,31]. Also, from these (111) peak positions, the lattice constants a of the Pt, Pd, and Pt–PdNPs are calculated to be 3.924, 3.894 and 3.899 Å, respectively. Assuming the Vegard's law holds for the Pt–PdNPs, these lattice constant values lead to an estimate of Pt/Pd = 1/4.9, deviating from both the nominal Pt/Pd ratio of 1/3 and EDS-determined value of 1/2.1 (Table S2), attributable to abundant defects and much stress involved in the Pt–PdNPs.

The TEM images of the Pt_1Pd_3NPs/G composite are shown in Fig. 2 with different magnifications. It is clearly observed that well-dispersed Pt–Pd alloy nanoparticles with an average size of 43 nm (Fig. S1) were successfully attached to the surfaces of the graphene sheets. The zoom-in image (Fig. 2B) shows that each Pt–Pd bimetallic nanoparticle is actually composed of many small nanoparticles with a size of approximately 4 nm. For the PtNPs/G and PdNPs/G composites, the average sizes of the Pt and Pd NPs, determined based on statistics of the TEM observation (Fig. S2), are 37 nm and 45 nm (Fig. S3), respectively, which are similar to the size of the Pt1–Pd3NPs loaded on graphene. The morphology of Pt–PdNPs/G appears similar to that of pure PtNPs/G while in contrast to that of PdNPs/G, probably due to a stronger electron acquisition ability of Pt vs Pd in the precursors, which predominates the initial nucleation as well as governs the further growth into complex nanoparticles for Pt–PdNPs/G.

Fig. 3 shows FE-SEM images of the Pt1Pd3NPs/G, including a secondary electron image (Fig. 3A) and a backscattered electron image (Fig. 3B). It is seen again that nanoparticles with uniform sizes are homogeneously distributed on the graphene sheets, consistent with the TEM observations. This demonstrates that the ascorbic acid used in this study can effectively reduce Pt and Pd ions to form Pt–Pd alloy nanoparticles on the graphene surface.

XPS was utilized to determine the surface elemental composition of the nanocomposites. Fig. 4A shows the C1s XPS spectrum of Pt1Pd3NPs/G. The spectrum indicates a considerable degree of oxidation of carbon with three components that correspond to carbon atoms in different functional groups: C–C (284.7 eV), C–O (286.7 eV) and O–C=O (288.9 eV) [32,33]. The peak intensity associated with C–C bonds indicates that the sp^2-hybridized graphitic structure is predominant in the graphene support. From the change of the intensity ratio of the C–C to C–O bonds (cf. Fig. S4), it is clear that the amount of C–O bonds decreased greatly after the chemical reduction by ascorbic acid, indicating effective reduction of the graphene oxide [34]. The Pt 4f and Pd 3d spectra of the sample are shown in Fig. 4B and C, respectively. The Pt 4f peaks in Fig. 4B can be deconvoluted into double peaks (71.8 eV and 75.2 eV) corresponding to metallic Pt $4f_{7/2}$ and Pt $4f_{5/2}$. Two peaks observed at 335.7 eV and 340.9 eV in Fig. 4C can be attributed to Pd $3d_{5/2}$ and Pd $3d_{3/2}$, respectively. These results confirm that the Pt and Pd precursors had been successfully reduced by ascorbic acid and formed Pt–Pd alloys anchored on the graphene sheets.

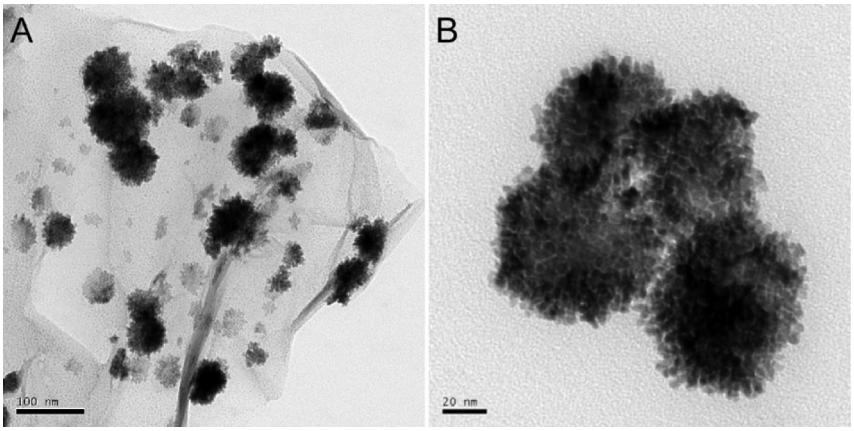

Fig. 2. TEM images of the Pt1Pd3NPs/G composites with different magnifications. The scale bars are 100 nm (left) and 20 nm (right), respectively.

3.2. Electrochemical characterizations of the Pt–PdNPs/G electrodes and analog nanocomposites

Cyclic voltammograms (CV) of the Pt-PdNPs/G electrodes were measured in 0.5 M H_2SO_4 compared to the electrodes made with analog nanocomposites such as PtNPs/G, PdNPs/G, Pt–PdNPs and Pt–PdNPs/V (Fig. 5). The experiments were performed at potentials between −0.2 and 1.2 V (*vs.* Ag/AgCl) with a scan rate of 100 mV s^{-1} at room temperature. The current peaks between −0.2 and 0.2 V are attributed to hydrogen adsorption and desorption, which is a useful element for evaluating the electrochemically active surface area (ECSA) of the catalyst. The anodic peaks during forward scanning and the cathodic peaks during reverse scanning are caused by the oxidation of metal and the reduction of metal oxide, respectively [35]. The ECSA value, which is the crucial factor affecting the electrocatalytic activity, can be evaluated by integrating the area under the CV curve in the hydrogen adsorption range after a double-layer correction [36]. With a value of 210 μC cm^{-2} for the adsorption of a monolayer of hydrogen atoms, the ECSA values of Pt1Pd3NPs/G, PtNPs/G, PdNPs/G, Pt1Pd3NPs and Pt1Pd3NPs/V are estimated to be 23.34, 21.93, 13.87, 18.96, and 23.69 m^2 g^{-1}, respectively. Pt–PdNPs/G has an ECSA value that is comparable with the one of Pt–PdNPs/V and obviously higher than those of, PtNPs/G, PdNPs/G and Pt–PdNPs, indicating its superior electrocatalytic activity towards the electro-oxidation of methanol.

3.3. Electrocatalytic properties of Pt–PdNPs/G and analog nanocomposites for the oxidation of methanol

The electrocatalytic activities of Pt–PdNPs/G and analog nanocomposites toward methanol oxidation were evaluated using cyclic voltammetry. The experiments were carried out using nitrogen saturated solutions of 1.0 M NaOH containing 0.5 M CH_3OH over a potential range of −0.9 to 0.4 V (*vs.* Ag/AgCl). In the following, we first report the results of Pt–PdNPs/G in comparison with graphene-supported monometallic nanocomposites (PtNPs/G and PdNPs/G) (Fig. 6) to reveal the bi-metallic effects on the electrocatalytic activity. Then, we compare Pt–PdNPs/G with free-standing and Vulcan-supported bi-metallic Pt–PdNPs composites in the oxidation of methanol (Fig. 7) to highlight the role of graphene in promoting the electrocatalytic performance.

In the electrocatalytic oxidation experiments applying all the catalysts, two alcohol oxidation peaks are observed as shown in Figs. 6A and 7A. The strong current peak in the forward scan is characteristic for methanol oxidation, which is assigned to the oxidation of freshly chemisorbed species coming from methanol adsorption [37]. The decrease of the current density at more positive potential was caused by the formation of Pt and Pd oxide, which hindered further chemisorptions of methanol. The reverse peak at −0.3 V was due to re-activating of the electrocatalytical surface for the oxidation of methanol, as a result of the reduction of Pt and Pd oxide in the negative scanning [38,39]. As seen in Fig. 6A, the Pt1Pd3NPs/G catalyst showed higher current density (2.727 mA cm^{-2}) than PtNPs/G (1.688 mA cm^{-2}) and PdNPs/G (1.157 mA cm^{-2}) did with a lower onset potential (−0.6 V vs −0.5 V for both PtNPs/G and PdNPs/G). This indicates that the electro-oxidation of methanol is easier to occur and proceeds faster on the surface of Pt–PdNPs/G than on surfaces of PtNPs/G and PdNPs/G.

The long-term electrocatalytic activity and stability are also key parameters for real applications of electrocatalysts. The electrocatalytic durability of PtNPs/G, PdNPs/G and Pt1Pd3NPs/G was

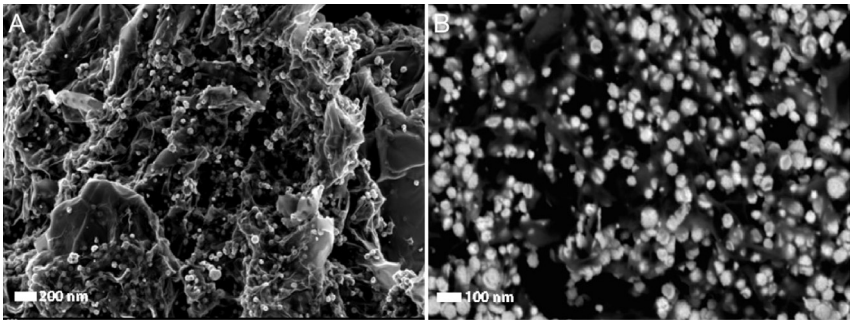

Fig. 3. Typical secondary electron image (A) and backscattered electron image (B) of the Pt1Pd3NPs/G composites.

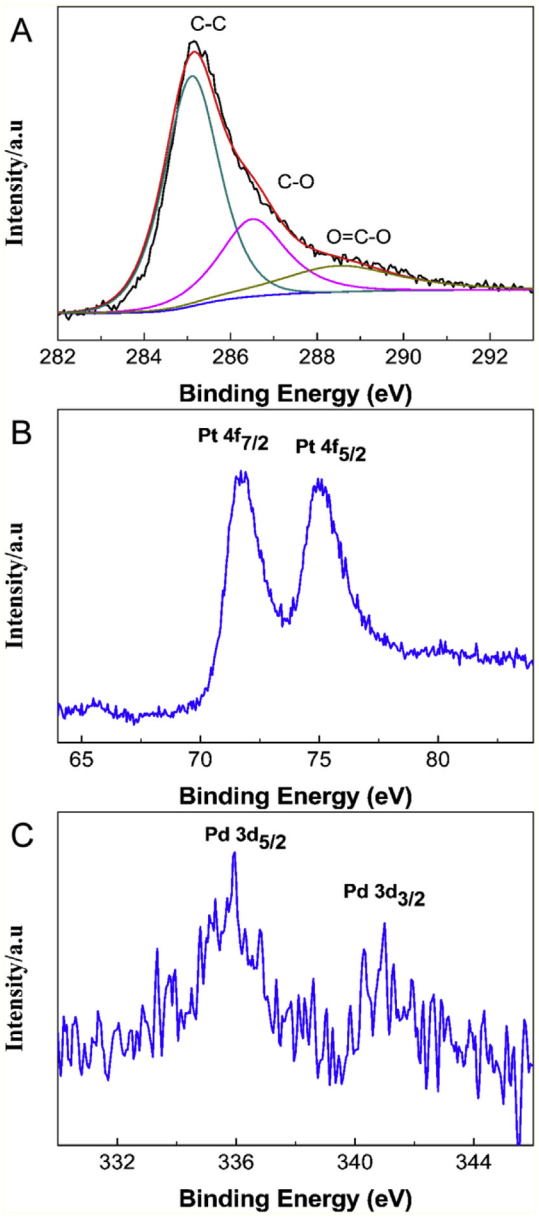

Fig. 4. Fine-scan XPS spectra of C 1s (A), Pd 4f (B) and Pd 3d (C) of the Pt1Pd3NPs/G composite.

examined using chronoamperometry with electrochemical oxidations of methanol for 700 s, as shown in Fig. 6B. Initially, a high current density was found for all catalysts due to the numerous active sites available on the surface of the catalysts. After about 20 s, the currents decayed rapidly due to the formation of CO-like intermediate carbonaceous species adsorbed on the active sites, preventing methanol from further oxidation on the surface of electrocatalysts [40]. The final current density of the Pt1Pd3NPs/G catalyst (0.464 mA cm^{-2}) is higher than that of PtNPs/G (0.196 mA cm^{-2}) and PdNPs/G (0.073 mA cm^{-2}), whereas the calculated current decline of Pt1Pd3NPs/G (79.44%) is lower than that of PtNPs/G (82.27%) and PdNPs/G (86.99%), suggesting that the alloy catalyst possesses much better poison tolerance during the electrochemical oxidation of methanol. As the activity for methanol oxidation greatly depends on the medium, the activities and stabilities of the different catalysts were also investigated in acidic environments. The experiments were carried out with nitrogen saturated solutions of 1.0 M H_2SO_4 containing 0.5 M CH_3OH over a potential range of 0.2–1.0 V (*vs.* Ag/AgCl). As shown in Fig. S5, Pt1Pd3NPs/G exhibits better electrocatalytic performance than PtNPs/G towards methanol oxidation even in the acidic condition. Compared to PtNPs/G and PdNPs/G, Pt–PdNPs/G shows superior electrocatalytic performance and stability during methanol oxidation, which demonstrates clearly the advantage of using bi-metals in the electrocatalysts involving metal nanoparticles. Considering Pt–PdNPs/G has a higher ECSA (23.34 m^2 g^{-1}) than PtNPs/G (21.93 m^2 g^{-1}) and PdNPs/G (13.87 m^2 g^{-1}), all with the same graphene support, the enhanced electrocatalytic performance of the bi-metallic nanocomposites should be mainly attributed to the increased ECSA resulting from the synergetic effects of the bi-metal NPs. In addition, it is indicated that the introduction of proper amount of Pd to alloy with Pt can overcome the poisoning effects of adsorbed CO-like species, and thus improve the electrocatalytic activities and tolerance towards methanol oxidation [21].

To further investigate the effects of the supporting materials on the electrocatalytic activities and tolerance of nanocomposites towards methanol oxidation, Pt–PdNPs loaded onto different supports (graphene, Vulcan-72 and no support) were evaluated using cyclic voltammetry and chronoamperometry. As shown in Fig. 7A, the peak current density of Pt1Pd3NPs/G (2.727 mA cm^{-2}) is higher than those of Pt1Pd3NPs (1.716 mA cm^{-2}) and Pt1Pd3NPs/V (1.821 mA cm^{-2}), demonstrating that the supporting material can substantially affect the electrocatalytic performance of the nanoparticles, As addressed in the introduction, graphene has exceedingly large specific surface area as well as high electronic conductivity. Considering both the Pt1Pd3NPs/G and Pt1Pd3NPs/V exhibit comparable ECSA (23.34 vs 23.69 m^2 g^{-1}), the superior electrocatalytic performance of Pt1–Pd3NPs/G relative to Pt1–Pd3NPs/V should be mainly attributed to the high electronic mobility of graphene, which enhances greatly the electron transfer during the electrocatalytic reaction [41]. For real applications of the electrocatalysts, the long-term electrocatalytic activity and stability are of great importance. The electrocatalytic durability of Pt1Pd3NPs, Pt1Pd3NPs/V and Pt1Pd3NPs/G were examined and the results are present in Fig. 7B. The calculated current decline of Pt1Pd3NPs/G (79.44%) is lower than that of Pt1Pd3NPs (91.53%) and Pt1Pd3NPs/V (85.46%). It suggests that the alloy catalyst possesses much better poison tolerance with graphene as the supporting material, again attributable enhanced electron transfer through graphene [21]. In addition, different electrodes prepared with the same Pt1Pd3NPs/G composite material were tested for methanol oxidation in alkaline solution, which all showed similar electrocatalytic behavior with a relative standard deviation (RSD) of only 1.46% (Table. S1). Moreover, the Pt1Pd3NPs/G modified electrodes showed fairly stable results after multiple cycles of voltammetry (Fig. S6). Both the multi-cycle reproducibility and long-term stability tests revealed satisfying performance of the Pt–PdNPs/G modified electrodes in the electro-oxidation of methanol.

In the following, the electrocatalytic performances of Pt–PdNPs/G catalysts with different Pt/Pd atomic ratios from 3/1 to 1/5 were investigated, in order to optimize the Pt/Pd atomic ratio for a best electrocatalytic performance. As shown in Fig. S7, the Pt–PdNPs in different Pt–PdNPs/G catalysts have similar average sizes of 40–50 nm. The actual Pt/Pd atomic ratios and the metal loading of the Pt–PdNPs/G catalysts were determined using EDS and TGA (Table S2), respectively. It is clearly seen that the actual Pt/Pd atomic ratios in the final Pt–PdNPs/G composites showed the same trend as the nominal Pt/Pd atomic ratios in the metal precursors from 3/1 to 1/5. Therefore, it is easy to control the Pt/Pd ratio in alloy nanoparticles by tuning the Pt/Pd ratio in the metal precursors. The metal loading of all Pt–PdNPs/G catalysts remained in the range of 60%–70%. Fig. 8 shows the cyclic voltammograms of

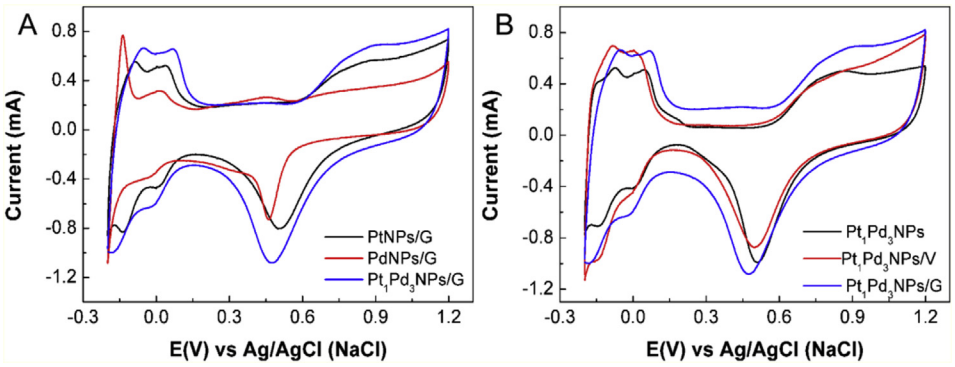

Fig. 5. Cyclic voltammograms of PtNPs/G (A), PdNPs/G (A), Pt1Pd3NPs/G (A, B), Pt1Pd3NPs (B), and Pt1Pd3NPs/V (B) in nitrogen saturated solutions of 0.5 M H_2SO_4 at a scan rate of 100 mV s^{-1}.

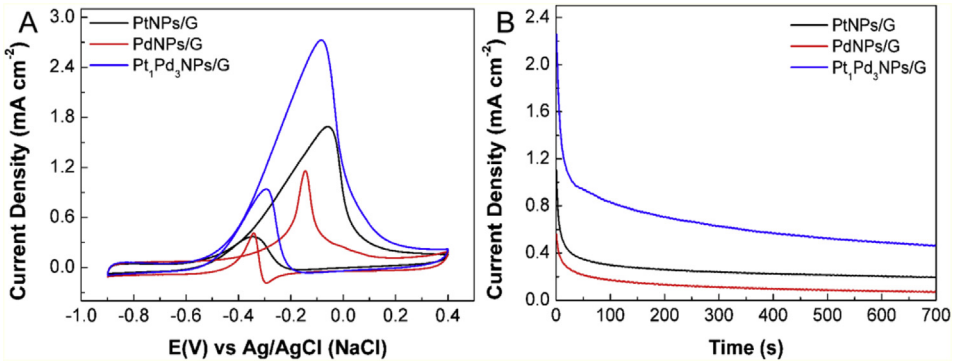

Fig. 6. Cyclic voltammograms (A) and chronoamperometric curves (B) of PtNPs/G, PdNPs/G, and Pt1Pd3NPs/G measured in nitrogen saturated solutions of 1.0 M NaOH containing 0.5 M CH_3OH at a scan rate of 100 mV s^{-1}.

methanol oxidations applying Pt–PdNPs/G electrodes with different nominal Pt/Pd ratios from 3/1 to 1/5. The experiments were carried out in nitrogen saturated solutions of 0.5 M CH_3OH in 1.0 M NaOH. The peak current densities of different Pt–PdNPs/G catalysts changed with the Pt/Pd ratio, and showed a maximum current density for the Pt–PdNPs/G catalyst with a nominal Pt/Pd ratio of 1/3. Therefore, the best electrocatalytic activity of Pt–PdNPs/G in an alkaline environment can be achieved with an optimized Pt/Pd ratio of 1/3, which may be attributable to the fact that a proper Pt–Pd ratio in Pt–PdNPs/G can minimize the poisoning of Pt during methanol electro-oxidation, as reported in the literature [42]. These results suggest that the synergistic effects of the Pt–Pd nanoparticles and the combination with graphene can lead to excellent electrocatalytic activity for the electro-oxidation of methanol, which is consistent with previous studies [21,43–45].

4. Conclusions

In summary, bimetallic Pt–Pd nanoparticles anchored on the graphene sheets were successfully synthesized using a simple, one-step method with ascorbic acid as the reductant. The as-prepared Pt–PdNPs/G nanocomposites combined the unique properties of graphene with alloying effects and showed superior electrocatalytic activity, satisfactory stability and high poisoning tolerance for the methanol electro-oxidation compared with graphene supported monometallic catalysts (PtNPs/G, PdNPs/G) and bimetallic

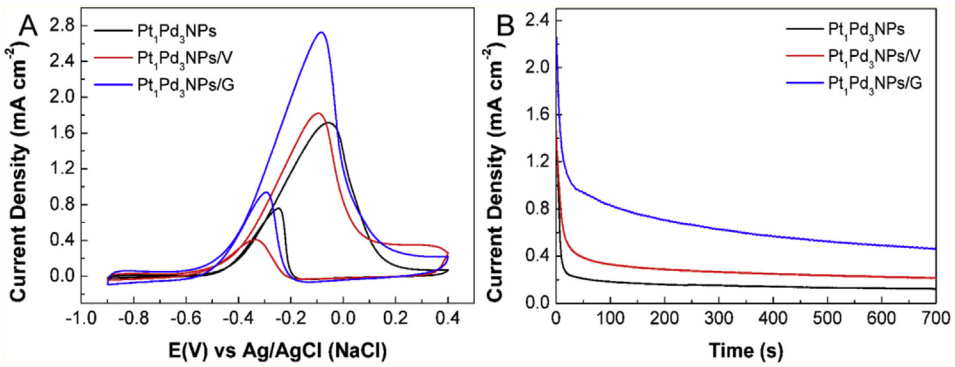

Fig. 7. Cyclic voltammograms (A) and chronoamperometric curves (B) of Pt1Pd3NPs, Pt1Pd3NPs/V, and Pt1Pd3NPs/G measured in nitrogen saturated solutions of 1.0 M NaOH containing 0.5 M CH_3OH at a scan rate of 100 mV s^{-1}.

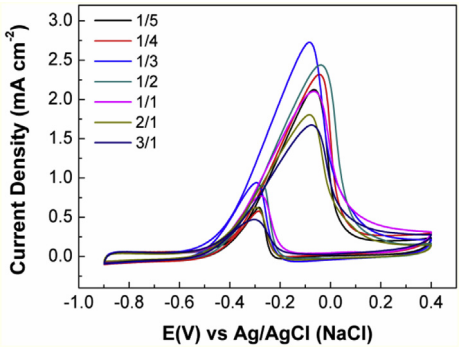

Fig. 8. Cyclic voltammograms of Pt–PdNPs/G with different Pt/Pd ratios in nitrogen saturated solutions of 1.0 M NaOH containing 0.5 M CH_3OH at a scan rate of 100 mV s^{-1}. The ratios from 1/5 to 3/1 represent the nominal Pt/Pd ratios in the initial metal precursors.

Pt–PdNPs with no or other carbon materials as support (Pt–PdNPs/Vulcan). In particular, the best electrocatalytic activity of Pt–PdNPs/G in an alkaline environment can be achieved with an optimized Pt/Pd ratio of 1/3. Considering the facile and controllable method for the preparation of Pt–PdNPs/G nanocomposites, this straightforward strategy may be applied to the development of other alloy–graphene nanocomposites as new electrode materials in Direct Methanol Fuel Cells.

Acknowledgments

This investigation was supported by the National Natural Science Foundation of China (Nos. 51102085, 61274010), Program for New Century Excellent Talents in University, Ministry of Education of China (NCET-09-0135), Natural Science Foundation of Hubei Province (Nos. 2011CDB057, 2011CDA81), Science Foundation from Hubei Provincial Department of Education (No. Q20111002), and Wuhan Municipal Academic Leaders Program (200951830550).

Appendix A. Supplementary data

Supplementary data related to this article can be found at http://dx.doi.org/10.1016/j.jpowsour.2014.03.127.

References

[1] C.Y. Wang, Chem. Rev. 104 (2004) 4727–4765.
[2] R.K. Ahluwalia, X. Wang, J. Power Sources 177 (2008) 167–176.
[3] H. Zhang, X. Xu, P. Gu, C. Li, P. Wu, C. Cai, Electrochim. Acta 56 (2011) 7064–7070.
[4] J.W. Guo, T.S. Zhao, J. Prabhuram, R. Chen, C.W. Wong, Electrochim. Acta 51 (2005) 754–763.
[5] A.N. Golikand, E. Lohrasbi, M.G. Maragheh, M. Asgari, J. Appl. Electrochem. 39 (2009) 2421–2431.
[6] C. Lamy, A. Lima, V. LeRhun, F. Delime, C. Coutanceau, J.M. Leger, J. Power Sources 105 (2002) 283–296.
[7] Q. Yuan, Z. Zhou, J. Zhuang, X. Wang, Chem. Commun. (Camb.) 46 (2010) 1491–1493.
[8] H. Zhang, Y.J. Yin, Y.J. Hu, C.Y. Li, P. Wu, S.H. Wei, C.X. Cai, J. Phys. Chem. C 114 (2010) 11861–11867.
[9] F. Kadirgan, S. Beyhan, T. Atilan, Int. J. Hydrogen Energy 34 (2009) 4312–4320.
[10] P. Waszczuk, G.Q. Lu, A. Wieckowski, C. Lu, C. Rice, R.I. Masel, Electrochim. Acta 47 (2002) 3637–3652.
[11] A.S. Arico, P.L. Antonucci, E. Modica, V. Baglio, H. Kim, V. Antonucci, Electrochim. Acta 47 (2002) 3723–3732.
[12] X. Zan, Z. Fang, J. Wu, F. Xiao, F. Huo, H. Duan, Biosens. Bioelectron. 49 (2013) 71–78.
[13] R. Feng, M. Li, J. Liu, Colloids Surf. A Physicochem. Eng. Asp. 406 (2012) 6–12.
[14] D. Basu, S. Basu, Int. J. Hydrogen Energy 36 (2011) 14923–14929.
[15] B. Molina Concha, M. Chatenet, Electrochim. Acta 54 (2009) 6130–6139.
[16] L. Chen, W. Zhao, Y. Jiao, X. He, J. Wang, Y. Zhang, Spectrochim. Acta Part A Mol. Biomol. Spectrosc. 68 (2007) 484–490.
[17] Y. Shu, L.E. Murillo, J.P. Bosco, W. Huang, A.I. Frenkel, J.G. Chen, Appl. Catal. A: Gen. 339 (2008) 169–179.
[18] Y. Hu, P. Wu, Y. Yin, H. Zhang, C. Cai, Appl. Catal. B: Environ. 111–112 (2012) 208–217.
[19] C. Hiromi, M. Inoue, A. Taguchi, T. Abe, Electrochim. Acta 56 (2011) 8438–8445.
[20] C.-F. Chi, M.-C. Yang, H.-S. Weng, J. Power Sources 193 (2009) 462–469.
[21] X. Yang, Q. Yang, J. Xu, C.-S. Lee, J. Mater. Chem. 22 (2012) 8057.
[22] F. Ksar, L. Ramos, B. Keita, L. Nadjo, P. Beaunier, H. Remita, Chem. Mater. 21 (2009) 3677–3683.
[23] N.G. Shang, P. Papakonstantinou, P. Wang, S. Ravi, P. Silva, J. Phys. Chem. C 114 (2010) 15837–15841.
[24] W. He, H. Jiang, Y. Zhou, S. Yang, X. Xue, Z. Zou, X. Zhang, D.L. Akins, H. Yang, Carbon 50 (2012) 265–274.
[25] J.D. Qiu, G.C. Wang, R.P. Liang, X.H. Xia, H.W. Yu, J. Phys. Chem. C 115 (2011) 15639–15645.
[26] K. Ji, G. Chang, M. Oyama, X. Shang, X. Liu, Y.B. He, Electrochim. Acta 85 (2012) 84–89.
[27] Y. Zhang, H. Shu, G. Chang, K. Ji, M. Oyama, X. Liu, Y.B. He, Electrochim. Acta 109 (2013) 570–576.
[28] Z. Liu, W. Xu, J. Fang, X. Xu, S. Wu, X. Zhu, Z. Chen, Appl. Surf. Sci. 259 (2012) 441–447.
[29] N.I. Kovtyukhova, P.J. Ollivier, B.R. Martin, T.E. Mallouk, S.A. Chizhik, E.V. Buzaneva, A.D. Gorchinskiy, Chem. Mater. 11 (1999) 771–778.
[30] X. Wang, J. Frenzel, W. Wang, H. Ji, Z. Qi, Z. Zhang, G. Eggeler, J. Phys. Chem. C 115 (2011) 4456–4465.
[31] C. Bianchini, P.K. Shen, Chem. Rev. 109 (2009) 4183–4206.
[32] S. Stankovich, D.A. Dikin, R.D. Piner, K.A. Kohlhaas, A. Kleinhammes, Y. Jia, Y. Wu, S.T. Nguyen, R.S. Ruoff, Carbon 45 (2007) 1558–1565.
[33] B. Jiang, C. Tian, L. Wang, Y. Xu, R. Wang, Y. Qiao, Y. Ma, H. Fu, Chem. Commun. (Camb.) 46 (2010) 4920–4922.
[34] Y. Li, W. Gao, L. Ci, C. Wang, P.M. Ajayan, Carbon 48 (2010) 1124–1130.
[35] Y.W. Lee, M. Kim, Y. Kim, S.W. Kang, J.H. Lee, S.W. Han, J. Phys. Chem. C 114 (2010) 7689–7693.
[36] S. Basri, S.K. Kamarudin, W.R.W. Daud, Z. Yaakub, Int. J. Hydrogen Energy 35 (2010) 7957–7970.
[37] Y.-H. Qin, H.-H. Yang, X.-S. Zhang, P. Li, C.-A. Ma, Int. J. Hydrogen Energy 35 (2010) 7667–7674.
[38] C. Lamy, J.M. Leger, J. Clavilier, R. Parsons, J. Electroanal. Chem. 150 (1983) 71–77.
[39] R. Parsons, T. Vandernoot, J. Electroanal. Chem. 257 (1988) 9–45.
[40] Y. Zhang, Y.-e. Gu, S. Lin, J. Wei, Z. Wang, C. Wang, Y. Du, W. Ye, Electrochim. Acta 56 (2011) 8746–8751.
[41] R. Kou, Y.Y. Shao, D.H. Wang, M.H. Engelhard, J.H. Kwak, J. Wang, V.V. Viswanathan, C.M. Wang, Y.H. Lin, Y. Wang, I.A. Aksay, J. Liu, Electrochem. Commun. 11 (2009) 954–957.
[42] Y. Zhang, G. Chang, S. Liu, J. Tian, L. Wang, W. Lu, X. Qin, X. Sun, Catal. Sci. Technol. 1 (2011) 1636.
[43] J.-J. Shi, G.-H. Yang, J.-J. Zhu, J. Mater. Chem. 21 (2011) 7343.
[44] X. Zhou, L. Fan, Electrochim. Acta 55 (2010) 8111–8115.
[45] A. Galal, N.F. Atta, H.K. Hassan, Int. J. Electrochem. Sci. 7 (2012) 768–784.